Supporting Information

Development of self-powered multicolored smart windows utilizing viologen derivatives

Wanxiong Yong,[a] Weining Liu,[a] Xiaoying Xin[a] and Guodong Fu*[a]

[a] School of Chemistry and Chemical Engineering, Southeast University

Email: 101010855@seu.edu.cn

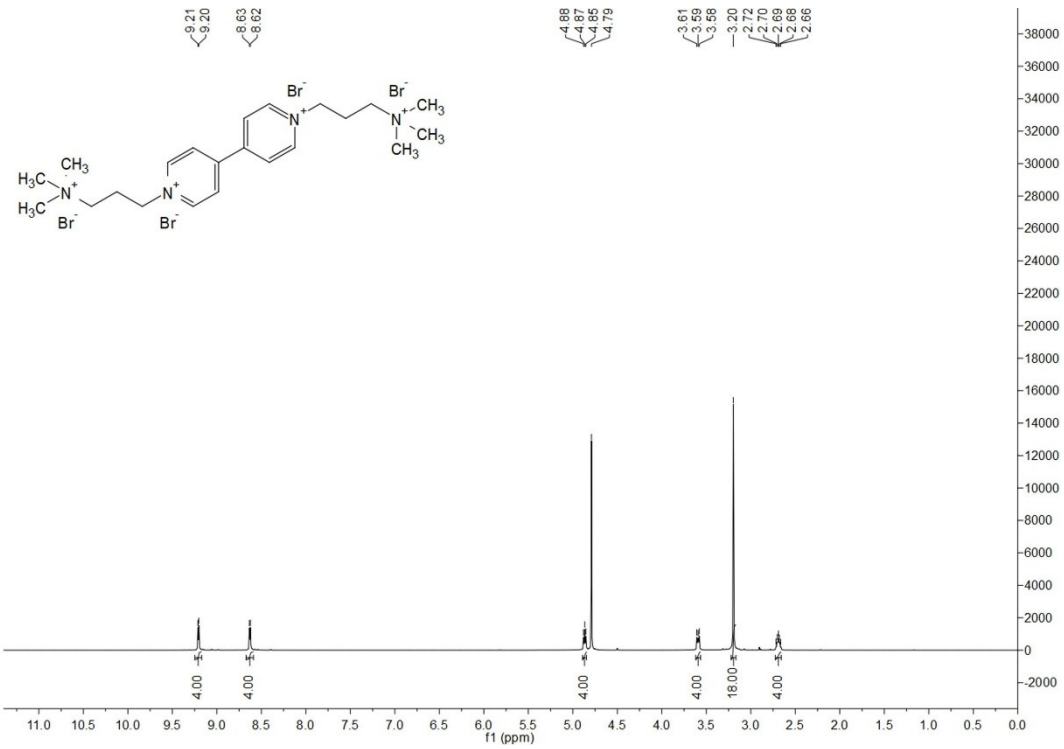

Fig. S1 ^{1}H-NMR spectra of 1,1'-bis(3-(trimethylammonio)propyl)-[4,4'-bipyridine]-1,1'-diium bromide (**V_1**).

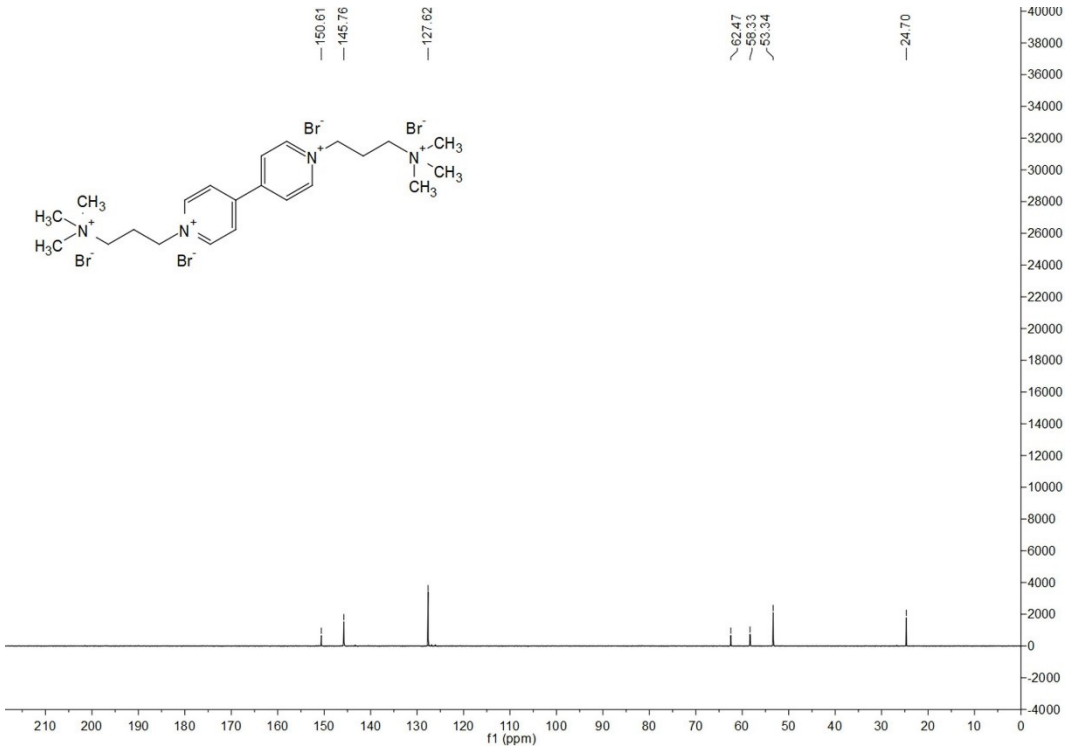

Fig. S2 ^{13}C-NMR spectra of 1,1'-bis(3-(trimethylammonio)propyl)-[4,4'-bipyridine]-1,1'-diium bromide (**V_1**).

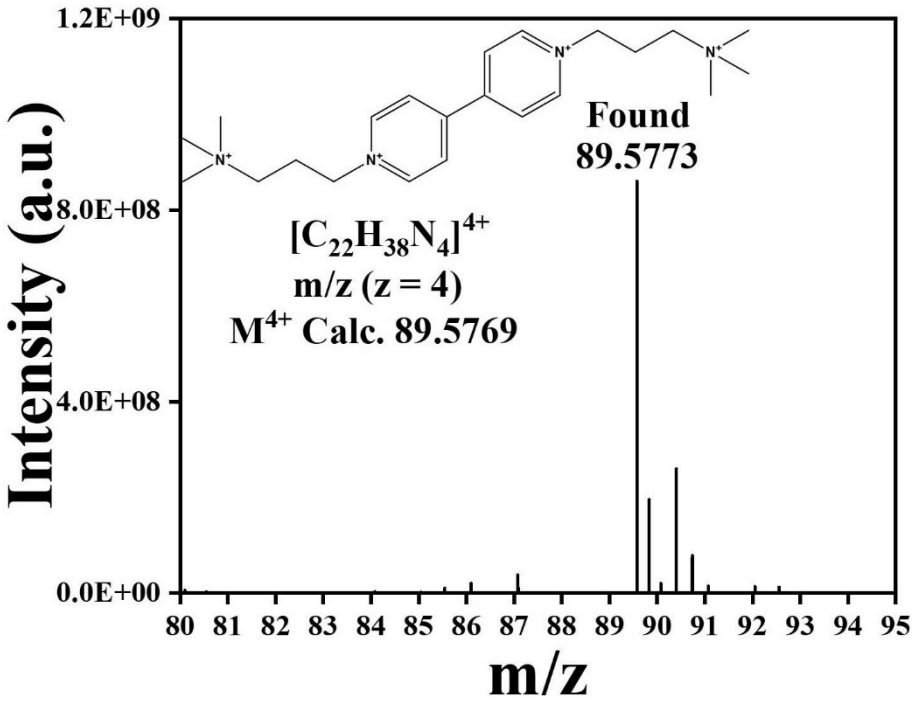

Fig. S3 HRMS (ESI) for $[C_{22}H_{38}N_4]^{4+}$ m/z (z = 4) M^{4+} calculated: 89.5769, found: 89.5773.

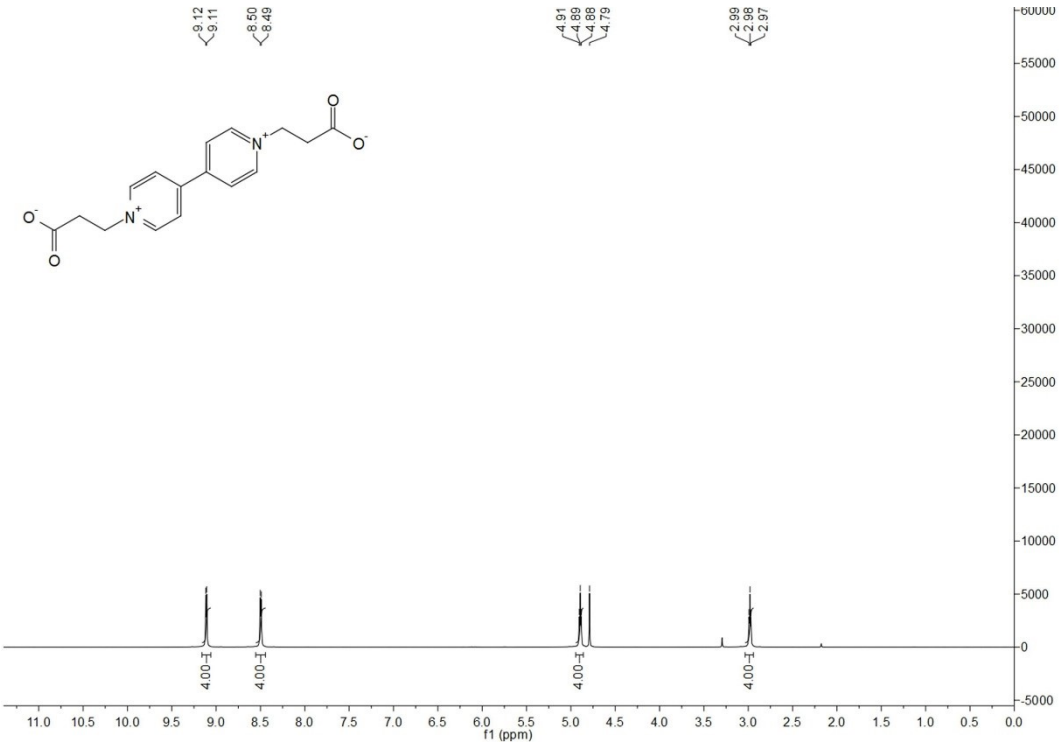

Fig. S4 ^{1}H-NMR spectra of 3,3'-([4,4'-bipyridine]-1,1'-diium-1,1'-diyl) dipropionate (**V_2**).

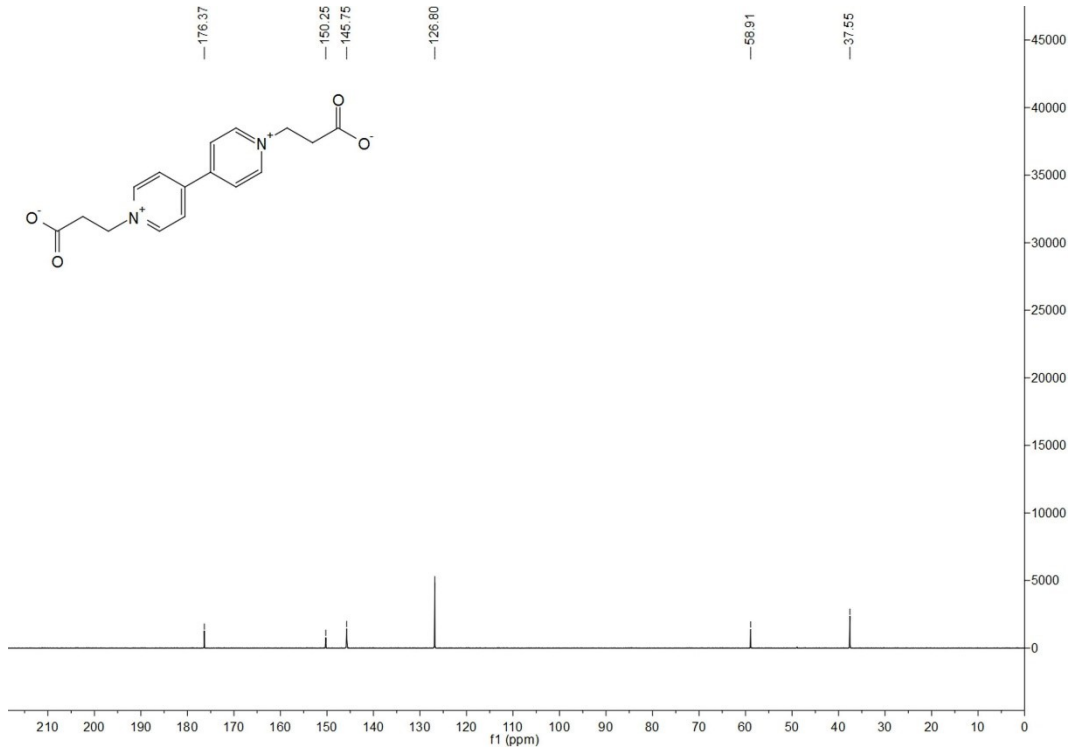

Fig. S5 ^{13}C-NMR spectra of 3,3'-([4,4'-bipyridine]-1,1'-diium-1,1'-diyl) dipropionate (**V_2**).

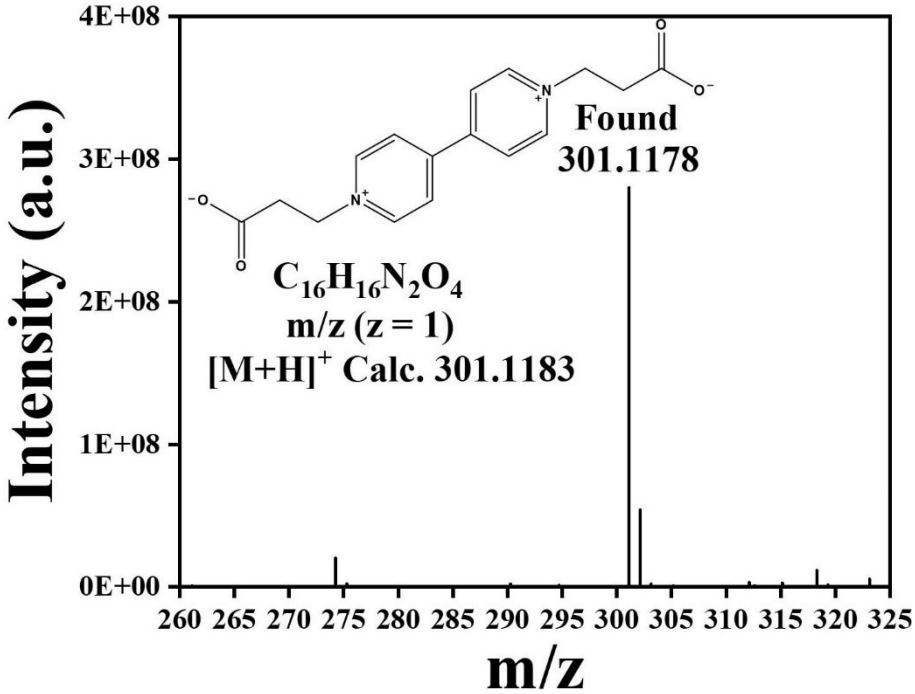

Fig. S6 HRMS (ESI) for $C_{16}H_{16}N_2O_4$ m/z (z = 1) $[M+H]^+$ calculated: 301.1183, found: 301.1178.

Fig. S7 ^{1}H-NMR spectra of 1,1'-bis(2,4-dinitrophenyl)-[4,4'-bipyridine]-1,1'-diium chloride (*p*-**V$_3$**)

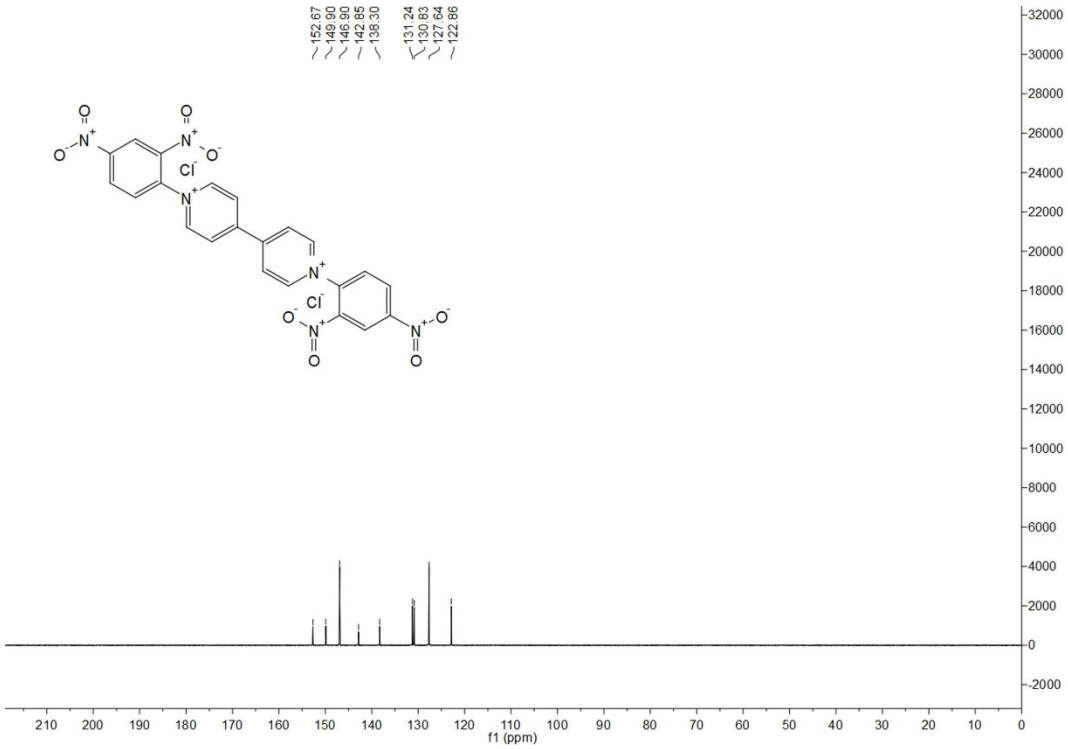

Fig. S8 ^{13}C-NMR spectra of 1,1'-bis(2,4-dinitrophenyl)-[4,4'-bipyridine]-1,1'-diium chloride (*p*-**V$_3$**)

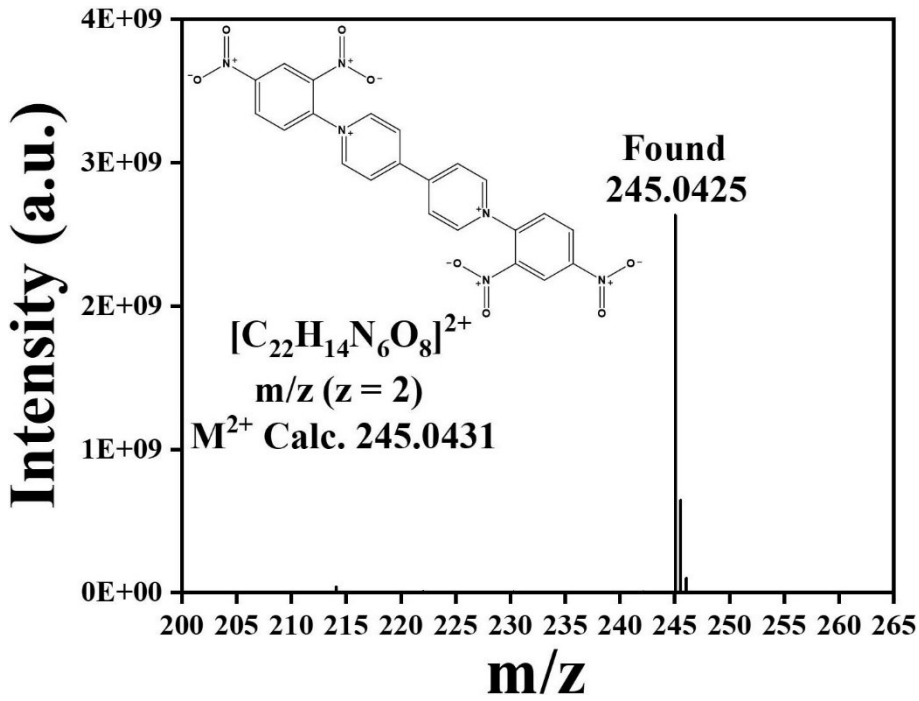

Fig. S9 HRMS (ESI) for $[C_{22}H_{14}N_6O_8]^{2+}$ m/z (z = 2) M^{2+} calculated: 245.0431, found: 245.0425.

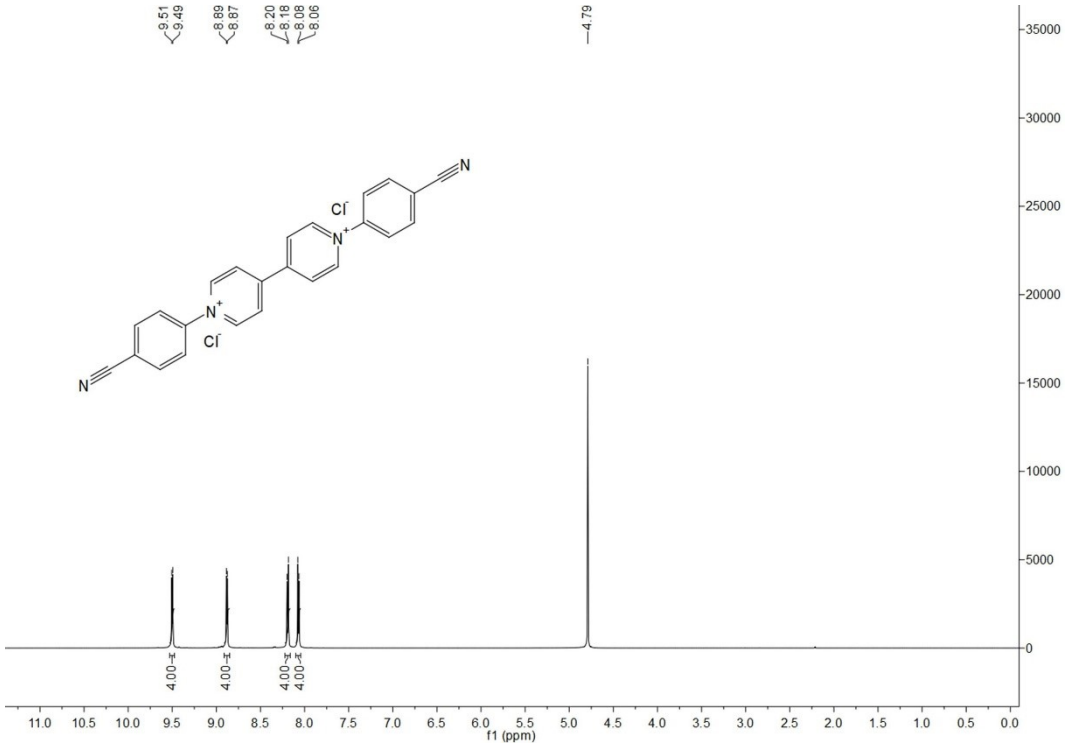

Fig. S10 ^{1}H-NMR spectra of 1,1'-bis(4-cyanophenyl)-[4,4'-bipyridine]-1,1'-diium chloride (**V_3**).

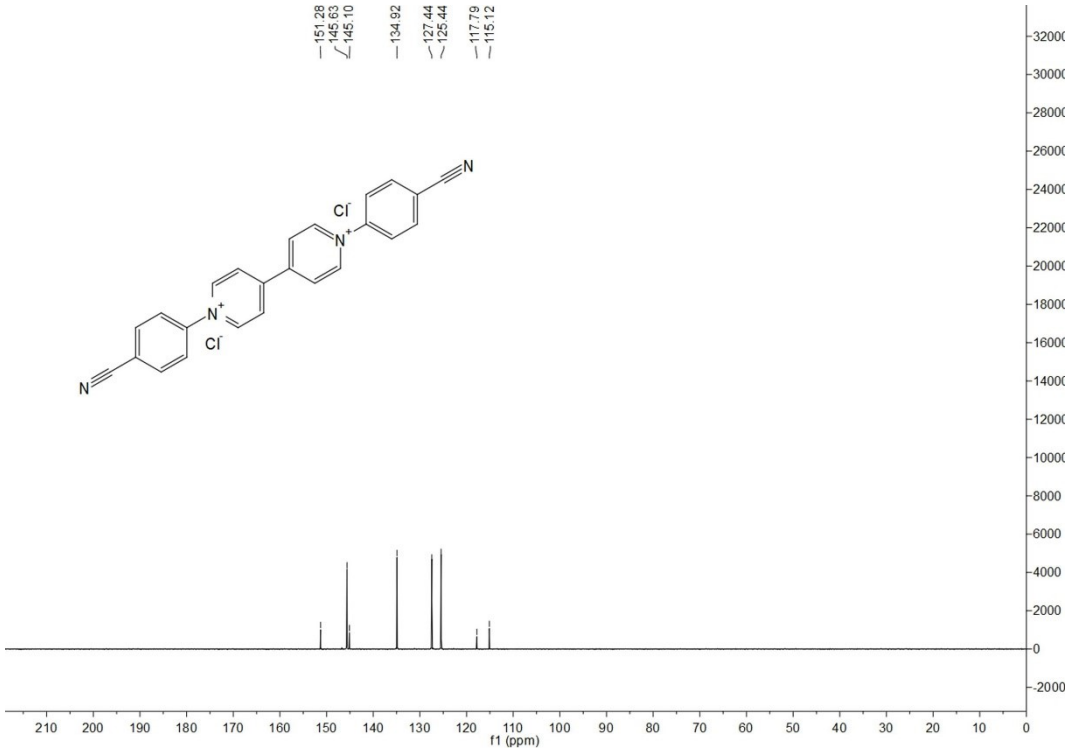

Fig. S11 ^{13}C-NMR spectra of 1,1'-bis(4-cyanophenyl)-[4,4'-bipyridine]-1,1'-diium chloride (**V_3**).

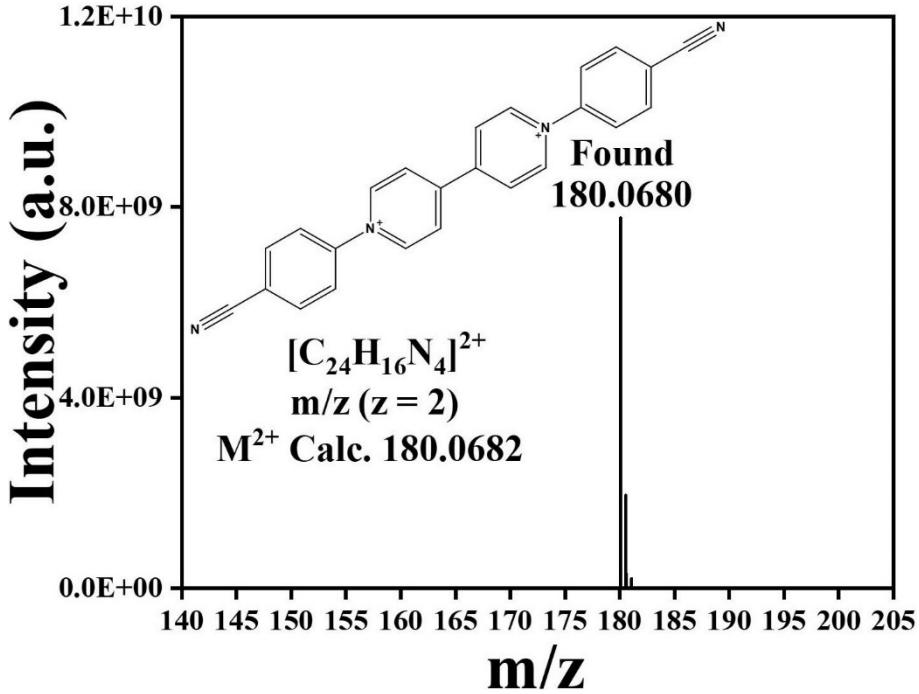

Fig. S12 HRMS (ESI) for $[C_{24}H_{16}N_4]^{2+}$ m/z (z = 2) M^{2+} calculated: 180.0682, found: 180.0680.

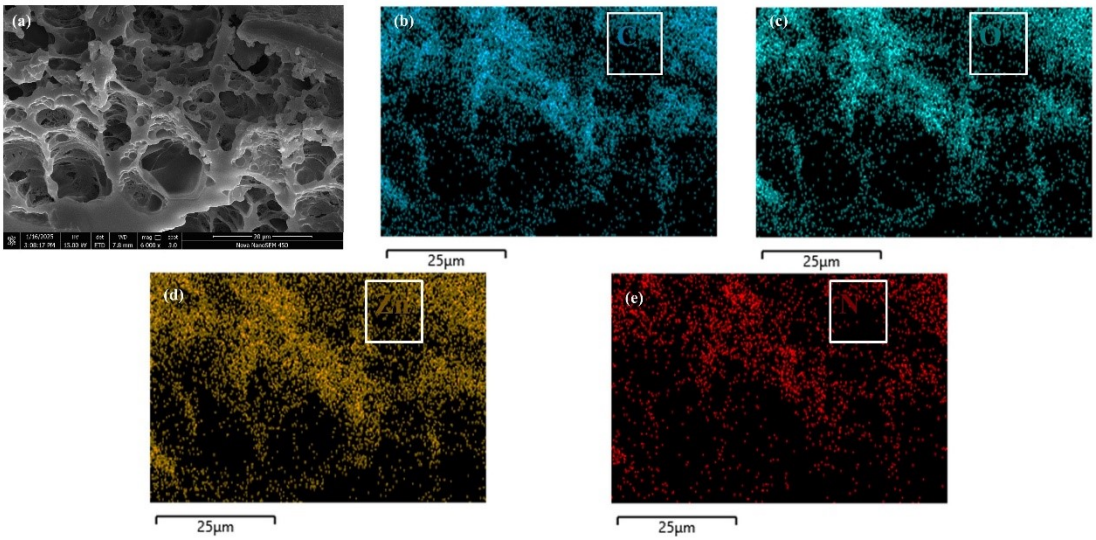

Fig. S13 (a) The SEM image of anode conductive gel; (b-e) images of element mapping of C, O, Zn and N of anode conductive gel.

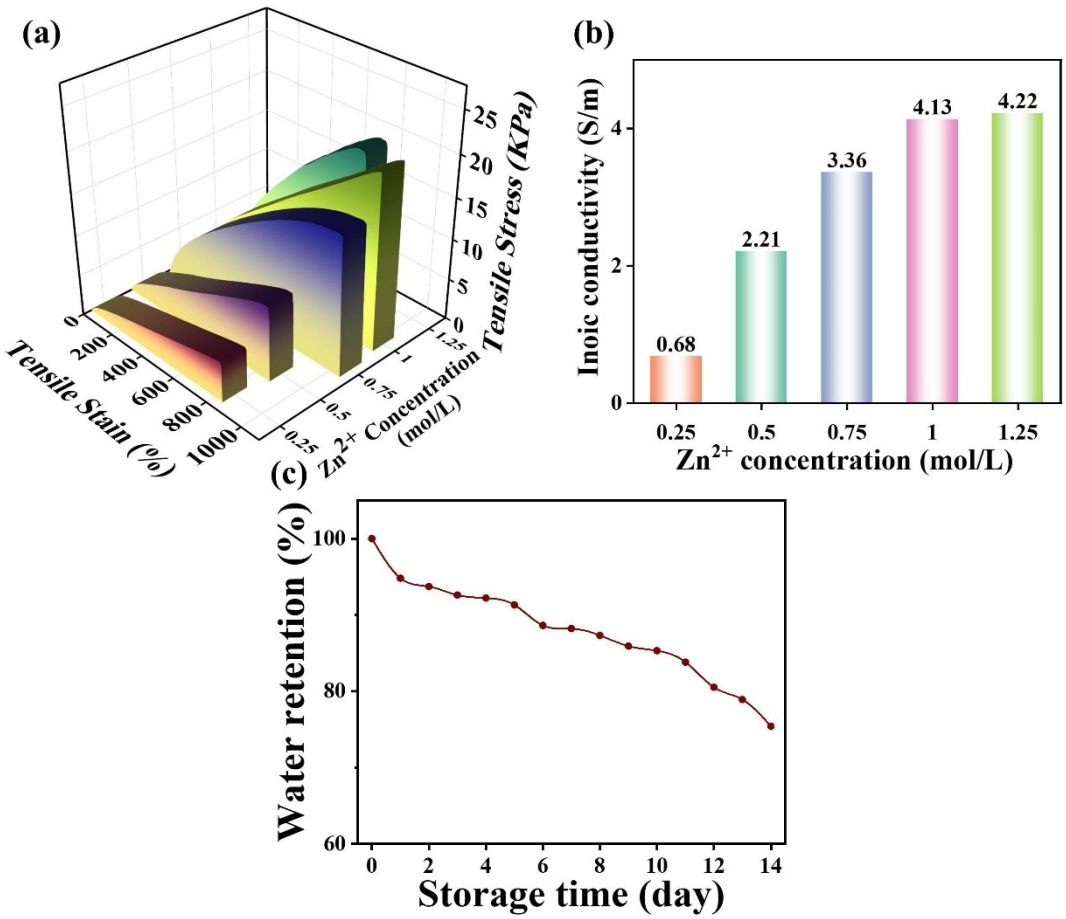

Fig. S14 Properties of the gel electrolyte (a) mechanical stability; (b) ion conductivity; (c) long-term stability.

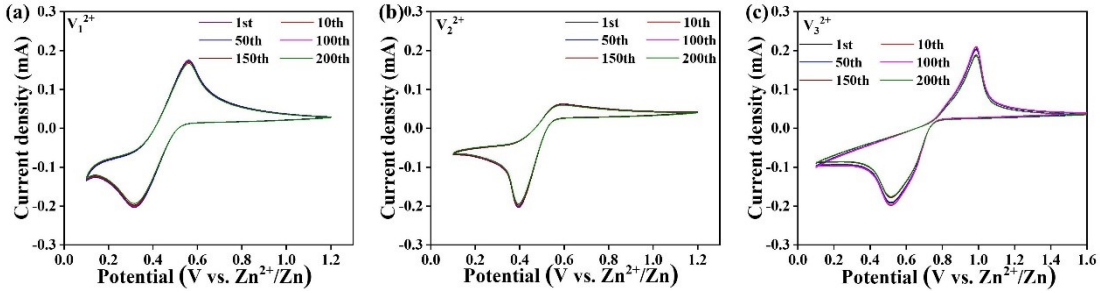

Fig. S15 (a-c) The cyclic CV curves of the $\mathbf{V_1}$, $\mathbf{V_2}$ and $\mathbf{V_3}$ devices.

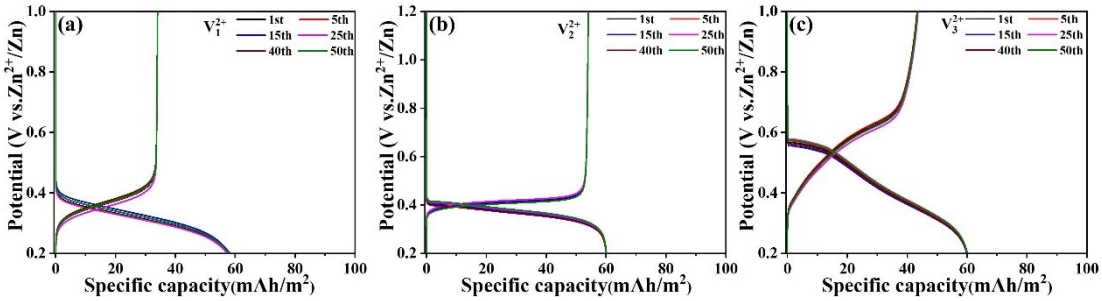

Fig. S16 (a-c) The cyclic GCD curves of the $\mathbf{V_1}$, $\mathbf{V_2}$ and $\mathbf{V_3}$ devices.

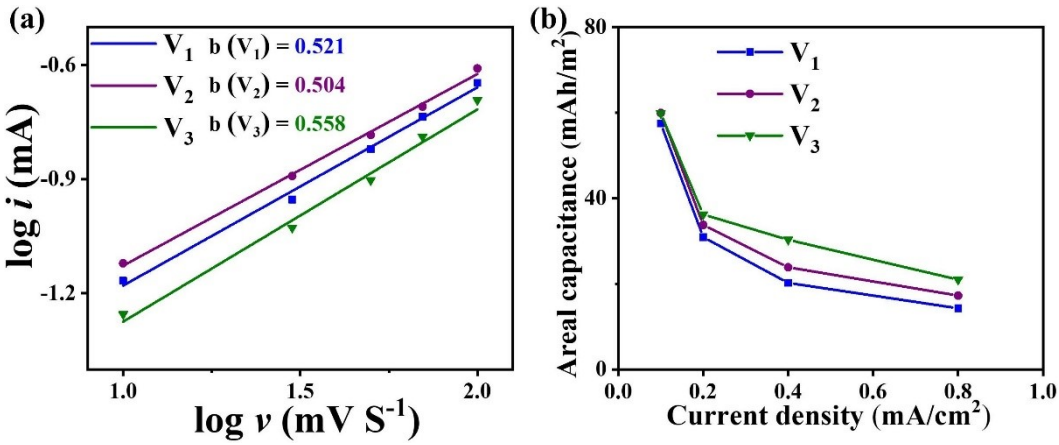

Fig. S17 (a) *b*-value of $\mathbf{V_1}$, $\mathbf{V_2}$ and $\mathbf{V_3}$ device; (b) Areal capacitance values through galvanostatic charge-discharge at different current rates.

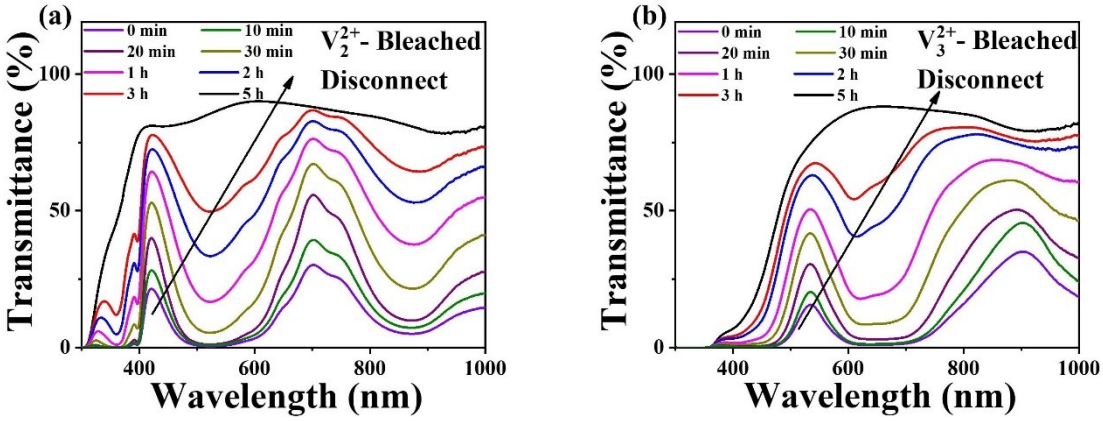

Fig. S18 (a, b) The transmittance at different moments of the $\mathbf{V_2}$ and $\mathbf{V_3}$ devices in the disconnecting process.

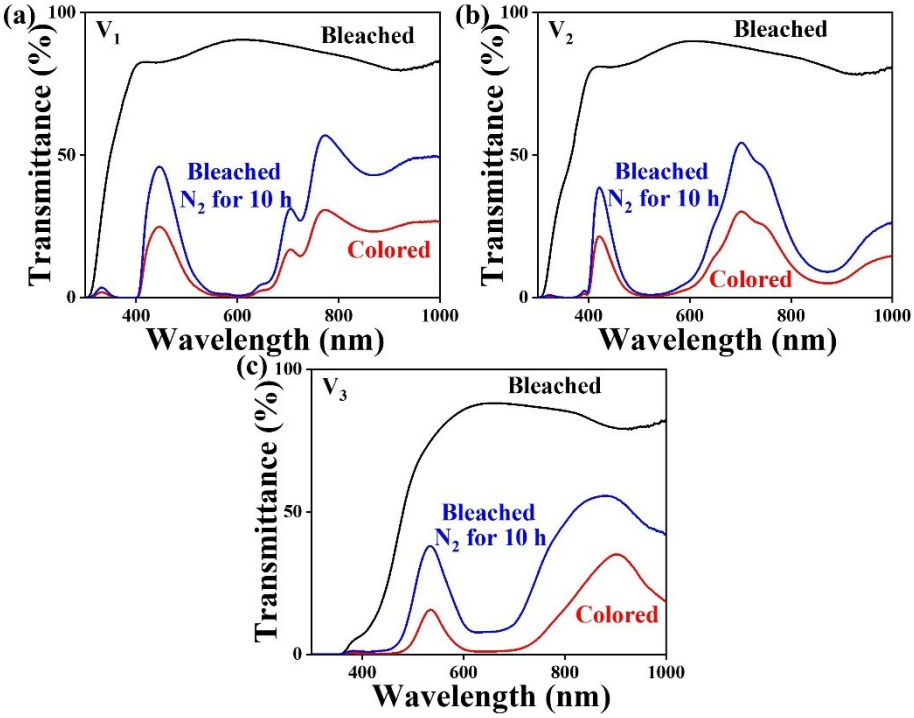

Fig. S19 (a), (b) and (c) The transmittance of the $\mathbf{V_1}$, $\mathbf{V_2}$ and $\mathbf{V_3}$ devices bleached for 10 h under N_2.

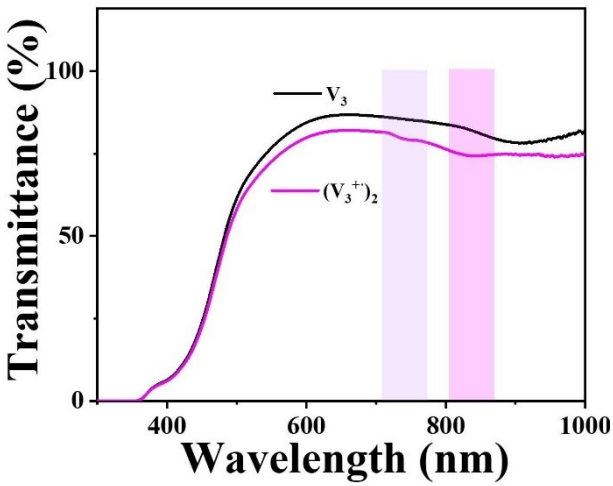

Fig. S20 (a) The transmittance of the initial $\mathbf{V_3}$ device and the transmittance observed after the formation of $(\mathbf{V_3}^{+\bullet})_2$ dimers.

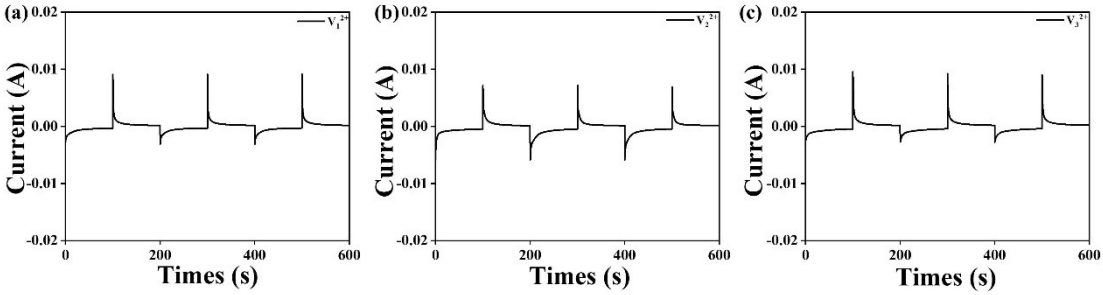

Fig. S21 The current-time curves: (a) $\mathbf{V_1}$ device; (b) $\mathbf{V_2}$ device; (c) $\mathbf{V_3}$ device.

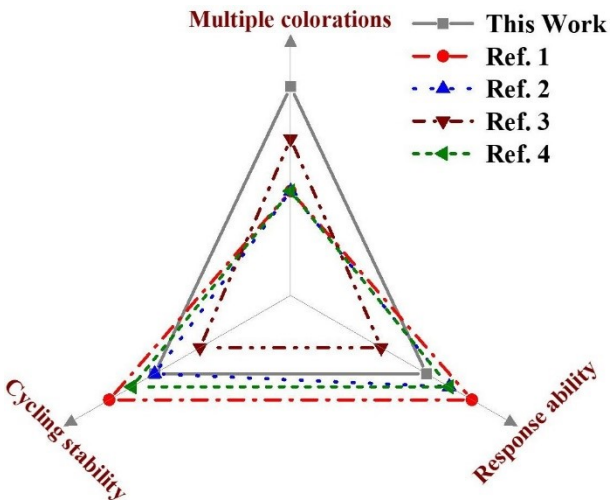

Fig. S22 Performance comparison of devices.

Ref:

[1] R. Roy, G. R, A. Basith, R. Banerjee and A. K. Singh, *Energy Storage Materials*, 2024, **71**, 103680.

[2] J. Du, C. Yue, Z. Zhang, Z. Liao, H. Tan, N. Li, J. Xu, Z. Tang and L. Xu, *Materials Today Chemistry*, 2023, **33**, 101658.

[3] C. Wang, Z. Wang, Y. Ren, X. Hou and F. Yan, *ACS Sustainable Chemistry & Engineering*, 2020, **8**, 5050-5055.

[4] B. Xu, J. Chen, P. Li, Y. Ouyang, Y. Ma, H. Wang and H. Li, *Nanoscale*, 2023, **15**, 19629-19637.